

Database-driven safe flight-envelope protection for impaired aircraft

Zhang, Ye; Huang, Yingzhi; Chu, Qiping; de Visser, Coen C.

DOI

[10.2514/1.1010846](https://doi.org/10.2514/1.1010846)

Publication date

2021

Document Version

Final published version

Published in

Journal of Aerospace Information Systems

Citation (APA)

Zhang, Y., Huang, Y., Chu, Q., & de Visser, C. C. (2021). Database-driven safe flight-envelope protection for impaired aircraft. *Journal of Aerospace Information Systems*, 18(1), 14-25.
<https://doi.org/10.2514/1.1010846>

Important note

To cite this publication, please use the final published version (if applicable).
Please check the document version above.

Copyright

Other than for strictly personal use, it is not permitted to download, forward or distribute the text or part of it, without the consent of the author(s) and/or copyright holder(s), unless the work is under an open content license such as Creative Commons.

Takedown policy

Please contact us and provide details if you believe this document breaches copyrights.
We will remove access to the work immediately and investigate your claim.



Database-Driven Safe Flight-Envelope Protection for Impaired Aircraft

Ye Zhang,* Yingzhi Huang,* Qiping Chu,[†] and Coen C. de Visser[‡]
Delft University of Technology, 2629HS Delft, The Netherlands

<https://doi.org/10.2514/1.1010846>

In this paper, an online flight envelope protection system is developed and implemented on impaired aircraft with structural damage. The whole protection system is designed to be a closed loop of several subsystems, including system identification, damage classification, flight-envelope prediction, and fault-tolerant control. Based on the information given by damage classification, the flight envelopes are explicitly retrieved, processed online from the database, and fed into the fault-tolerant controller, which makes the protection system adaptive to a wide range of abnormal conditions. Simulation results show that with envelope protection, loss-of-control accidents are more likely to be prevented, since excessive commands to the controller are restricted based on the updated information of the changed flight envelopes. In this way, the fault tolerance of the impaired aircraft can be effectively enhanced.

I. Introduction

LOSS-OF-CONTROL (LOC) prevention by means of flight-envelope protection has seen much attention recently. The function of a flight-envelope protection system is twofold: an augmentation of the flight controller to monitor and maintain the aircraft within its flight envelope [1–3], and an auxiliary system to inform pilots of the current flight envelopes via human–machine interactions such as haptics and visual displays [4–7]. The first function prevents pilots from oversteering the aircraft by limiting the commands to the flight controller, and the second function directly provides safety-related information to the pilots so that they can make unconventional control strategies without violating the envelope boundaries. These two functions work in cooperation to enhance the flight safety. In this paper, our research mainly focuses on the first function.

Due to convoluted contributing factors to LOC accidents, it is hardly possible to give a holistic solution. Among various causal factors of LOC accidents, structural damage has received some attentions. In Ref. [8], the proposed control and guidance algorithms are validated on unmanned aircraft under severe structural damage. In Ref. [9], identification and control algorithms were applied to a Boeing 747 aircraft based on real accident scenarios including wing damage. Although these research works did not focus on the usage of flight-envelope protection, they have shown the important and potential of integrating flight-envelope information into flight controllers.

Most flight-envelope protection systems are designed for specific situations and purposes, based on flight envelopes of various definitions and forms. In Ref. [10], five LOC envelopes are proposed as the criterion to predict LOC accidents. By mapping flight-test data (including stall) and LOC accident data into these flight envelopes, LOC events can be characterized and predicted by excursions outside at least three of these envelopes [11]. Based on these flight envelopes, a flight-envelope protection scheme is developed in Refs. [1,12] on a

command-limiting architecture and is designed to augment a standard gain-scheduled flight control law. In Ref. [13], a trim database was developed to define the postdamage flight envelope for adaptive flight planning. A sequence of trim conditions can be determined by the planner and safely followed by the aircraft, which is also used in the envelope-aware flight management system proposed in Ref. [14]. Again, flight envelopes defined in Ref. [10] are used for flight safety assessment and management.

The aforementioned flight envelopes indicate the hard limits of the aircraft. Sometimes, it is of equal importance to investigate how aircraft can maneuver to and from LOC envelopes or trim envelopes, especially under failures and damage conditions. Therefore, in our research work, we calculate the flight envelope as a subset of the hard-limit envelopes using reachability analysis defined and proposed in Refs. [15–17]. One advantage of this technique is that all possible trajectories can be computed from all available control strategies and initial states, which naturally meets the safety guarantees [18]. Compared with similar work that also discussed reachability-based flight envelopes [19,20], work by Zhang et al. [21,22] on flight-envelope prediction considerably reduces the computational burden and circumvents many complications related to online calculation of flight envelopes. As a follow-up of previous research, this paper proposed a flight-envelope protection system that for the first time integrates reachability-based flight envelopes into a fault-tolerant controller to reach the goal of LOC prevention.

This work is the integration of different modules that were separately developed in previous papers so that a complete loop is formed to solve practical damage cases. This paper also contributes to a procedure to generate a safe level of excitation inputs for system identification in abnormal situations, which aims to achieve a balance between safety and accuracy. Offline analysis and online simulations enable models and envelopes in the database to be fully validated and verified for structural-damage cases. The simulations are conducted in near-real time, which shows the feasibility of onboard applications of the proposed system.

II. Online Implementation

The implementation of a flight-envelope prediction system (which includes system identification, fault/damage diagnosis, and database building) has been thoroughly discussed in Refs. [21,22]. However, none of these have practical meaning if they are not connected and running in the loop with an automatic fault-tolerant controller (FTC). Figure 1 shows the complete flight-envelope protection system, which combines previously developed modules of envelope prediction together with an FTC. In this way, commands from pilot/autopilot as well as flight states can be constrained within the new flight envelope in abnormal situations.

Presented as Paper 2020-1374 at the AIAA SciTech 2020 Forum, Orlando, FL, January 6–10, 2020; received 19 March 2020; revision received 21 September 2020; accepted for publication 22 September 2020; published online 11 November 2020. Copyright © 2020 by The Authors. Published by the American Institute of Aeronautics and Astronautics, Inc., with permission. All requests for copying and permission to reprint should be submitted to CCC at www.copyright.com; employ the eISSN 2327-3097 to initiate your request. See also AIAA Rights and Permissions www.aiaa.org/randp.

*Ph.D. Student, Control and Simulation Section, Faculty of Aerospace Engineering, Kluyverweg 1; currently Lecturer, University of Shanghai for Science and Technology, 516 Jungong Rd., Shanghai, China. Member AIAA.

[†]Associate Professor, Control and Simulation Section, Faculty of Aerospace Engineering, Kluyverweg 1. Member AIAA.

[‡]Assistant Professor, Control and Simulation Section, Faculty of Aerospace Engineering, Kluyverweg 1. Member AIAA.

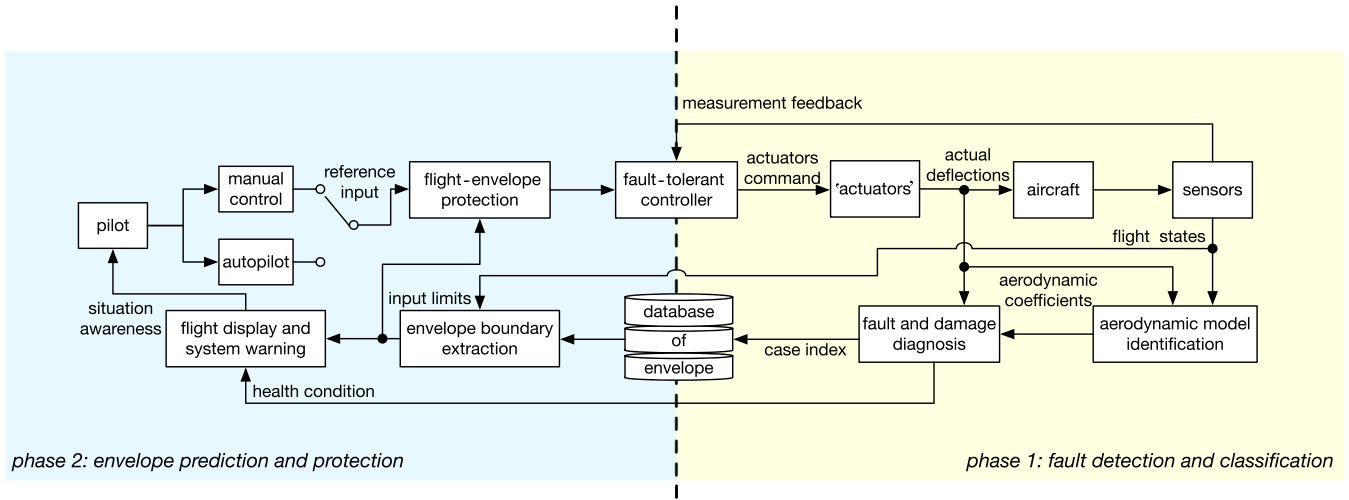


Fig. 1 An overview of the complete loop to be implemented online.

What we are focusing on are “potentially” catastrophic situations, where LOC is likely to happen if maneuvers are initiated without knowledge of the current abnormal condition and reduced flight envelopes. In these cases, it is still possible to control the aircraft given sufficient control authority and maneuverability based on the updated flight envelope. The protection system proposed in this paper thus plays an important role in preventing impaired aircraft from entering LOC conditions after a sudden change in the system dynamics and control authorities, as well as turning them into survivable incidents.

The flight after faults/damage can be divided into two phases. During the first phase, the initial trim condition is disturbed by sudden faults/damage and the aircraft is quickly restabilized by the onboard FTC if sufficient control authority is available. The quick reaction of the controller alleviates the work load of pilots so that they can focus more on situation analysis and higher-level decision-making.

Meanwhile, the detection alarm is triggered, which starts the reidentification of the aerodynamic model. The availability of persistent excitation inputs is one of the key issues in model identification. In abnormal situations, aircraft are more likely to lose control during maneuvering. Hence, excitation inputs, if required, should be given with safety considerations. However, a significant challenge is to decide the scale of identification inputs before diagnosis information is provided. In most literature, excitation inputs are given based on pilot experience and intuitions, which in the case of failures can pose a large potential risk. In this paper, we propose to quantify the scale of excitation inputs by first retrieving the most conservative flight envelope in the database, and then adding incremental inputs when more diagnosis information flows in. The retrieved flight envelope is used to determine how small the inputs should be in order to reduce the risk of LOC.

One issue with this constrained excitation is that limited inputs may give inaccurate identification results. The lack of accuracy can be compensated for by the high generalization ability of well-trained classifiers used in the diagnosis system [21]. Hence, the priority can be given to safety while the fidelity of diagnosis can be maintained, even when model identification is compromised. In this way, the system identification and diagnosis system provide information on the current abnormal situation of the aircraft as well as the reduced control authorities, which generate a match with a case index to one flight envelope in the database.

The second phase starts when the aircraft attempt to conduct large amplitude maneuvers (e.g., turning, ascending, descending). If the maneuver command is given without considering the changed envelopes, the aircraft may fly into unrecoverable states. It will be shown in the simulation example that excessive inputs may generate incremental moments that cannot be counteracted given the remaining

control authorities, leading to the saturation of actuators and LOC. Therefore, flight envelopes retrieved from the database are incorporated in the control and warning system to protect the aircraft from LOC situations. In this way, within the remaining maneuverability, the envelope protection system can help the pilots to safely maneuver and eventually land the aircraft after sudden damage.

III. Reconfiguration of Flight Controls

A fault-tolerant controller is designed to reconfigure the flight control laws when there are system faults and damage. The reconfigured controller is expected to achieve the control objective by using remaining control effectiveness or alternate control surfaces to adapt to the changed system dynamics and mitigate the adverse impact of faults and damage. A comprehensive review of FTCs and their comparisons can be found in Refs. [23,24].

Among various adaptive fault-tolerant control methods for nonlinear systems, the incremental nonlinear dynamic inversion (INDI) control [25,26] has been intensively applied to different types of aircraft. The INDI method can be considered as an incremental form of the widely used feedback linearization approach [9,27]. The advantage of the INDI method is that it makes the controller significantly less sensitive to model mismatch with simpler control design. In situations of airframe structural damage, the presence of model mismatch is inevitable. The INDI method uses sensor information to replace a large part of the model, including its unmodeled uncertainties, making it much less model dependent and very suitable for fault-tolerant control. In practice, the high performance and adaptiveness of the INDI controller has been proved by many published results from simulations as well as real-world flight tests [26,28–33].

In this paper, the flight-envelope protection can be implemented through the INDI flight controller to ensure that the aircraft stays within the state boundaries of flight envelopes. By applying the command-limiting strategy [34], the envelope limits can be mapped onto command limits that are enforced into the controller.

The aircraft is controlled in a multiloop structure based on its dynamics model. In abnormal situations, maintaining control of attitude and aerodynamic angles is the primary concern. As illustrated in Fig. 2, the control law consists of two loops: an outer loop for control of the roll angle ϕ , angle of attack α , and sideslip angle β ; and an inner loop for the control of the roll, pitch, and yaw angular rates represented by the vector $\omega = [p, q, r]^T$. The engine throttle is controlled by a separated autothrottle loop to maintain a commanded airspeed. The commands for ϕ , α , and β (represented in Fig. 2 by the vector $[\phi, \alpha, \beta]_{\text{ref}}$) and that for airspeed (represented by V_{ref} in Fig. 2) are set by the pilots/autopilot. The dynamics of $[\phi, \alpha, \beta]^T$ can be written in the form [35]

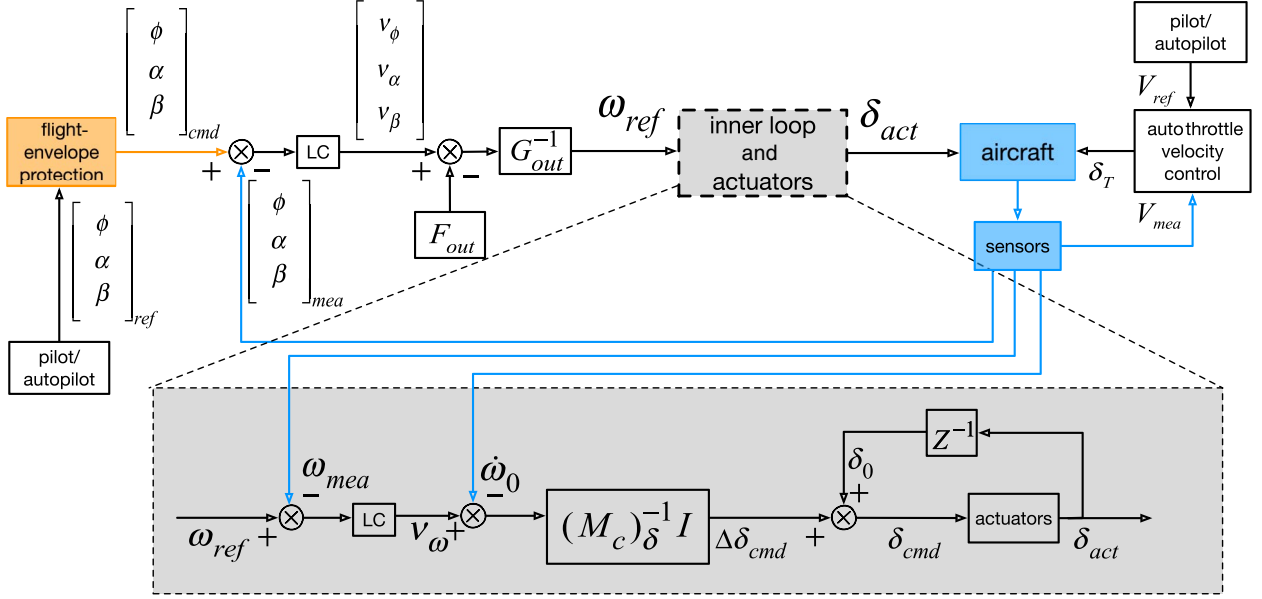


Fig. 2 Multiloop NDI/INDI control structure.

$$\begin{bmatrix} \dot{\phi} \\ \dot{\alpha} \\ \dot{\beta} \end{bmatrix} = F_{\text{out}} + G_{\text{out}} \boldsymbol{\omega} = \begin{bmatrix} 0 \\ f_{\alpha} \\ f_{\beta} \end{bmatrix} + \begin{bmatrix} 1 & \sin \phi \tan \theta & \cos \phi \tan \theta \\ \frac{-uv}{u^2 + w^2} & 1 & \frac{-vw}{u^2 + w^2} \\ \frac{w}{\sqrt{u^2 + w^2}} & 0 & -\frac{u}{\sqrt{u^2 + w^2}} \end{bmatrix} \begin{bmatrix} p \\ q \\ r \end{bmatrix} \quad (1)$$

where

$$f_{\beta} = \frac{1}{\sqrt{u^2 + w^2}} \left[-\frac{uv}{V^2} (A_x - g \sin \theta) + \left(1 - \frac{v}{V^2} \right) (A_y + g \sin \phi \cos \theta) - \frac{vw}{V^2} (A_z + g \cos \phi \cos \theta) \right] \quad (2)$$

$$f_{\alpha} = \frac{1}{u^2 + w^2} [u(A_z + g \cos \phi \cos \theta) - w(A_x - g \sin \theta)] \quad (3)$$

and A_x , A_y , and A_z denote the specific forces along the body X/Y/Z axis; u , v , and w are the velocity components along the body X/Y/Z axis. The values of these states as well as the Euler angles are measured from onboard sensors.

Since Eqs. (1) and (2) contains no model uncertainty, a classic nonlinear dynamic inversion (NDI) controller is applied to the outer loop. The desired input to the inner-loop control $\boldsymbol{\omega}_{\text{ref}} = [p, q, r]_{\text{ref}}^T$ is solved by introducing a virtual input vector $[\nu_{\phi}, \nu_{\alpha}, \nu_{\beta}]^T$ to the outer-loop controller:

$$\boldsymbol{\omega}_{\text{ref}} = G_{\text{out}}^{-1}([\nu_{\phi}, \nu_{\alpha}, \nu_{\beta}]^T - F_{\text{out}}) \quad (4)$$

Substituting Eq. (4) into the dynamics equation Eq. (1) yields a decoupled linear relation:

$$[\dot{\phi}, \dot{\alpha}, \dot{\beta}]^T = [\nu_{\phi}, \nu_{\alpha}, \nu_{\beta}]^T \quad (5)$$

Therefore, the virtual input $[\nu_{\phi}, \nu_{\alpha}, \nu_{\beta}]^T$ can be solved by a linear controller (LC), as shown in Fig. 2.

The resulting $\boldsymbol{\omega}_{\text{ref}}$ is used for controlling the inner loop of angular rates, where the Euler equations of motion are used [26]:

$$\boldsymbol{M} = \boldsymbol{I} \dot{\boldsymbol{\omega}} + \boldsymbol{\omega} \times \boldsymbol{I} \boldsymbol{\omega} \quad (6)$$

where $\boldsymbol{M} = [L, M, N]^T$ are the angular moments acting on the aircraft, and the inertia matrix is denoted by \boldsymbol{I} .

The moments \boldsymbol{M} can be specified as a combination of flight-states-related moments \boldsymbol{M}_a generated by airframe aerodynamics with zero control surfaces deflection, and \boldsymbol{M}_c is generated by the control surfaces' deflections. Solving the preceding equation for $\dot{\boldsymbol{\omega}}$ yields [26]

$$\dot{\boldsymbol{\omega}} = \boldsymbol{I}^{-1}(\boldsymbol{M}_a + \boldsymbol{M}_c - \boldsymbol{\omega} \times \boldsymbol{I} \boldsymbol{\omega}) \quad (7)$$

by assuming the linear control surfaces' ($\boldsymbol{\delta} = [\delta_a, \delta_e, \delta_r]^T$) aerodynamic effectiveness, which is

$$\boldsymbol{M}_c = (\boldsymbol{M}_c)_{\boldsymbol{\delta}} \boldsymbol{\delta} = \frac{1}{2} \rho V^2 S \begin{bmatrix} bC_{l_{\delta a}} & 0 & bC_{l_{\delta r}} \\ 0 & \bar{c}C_{m_{\delta e}} & 0 \\ bC_{n_{\delta a}} & 0 & bC_{n_{\delta r}} \end{bmatrix} \begin{bmatrix} \delta_a \\ \delta_e \\ \delta_r \end{bmatrix} \quad (8)$$

where $(\boldsymbol{M}_c)_{\boldsymbol{\delta}} = (\partial/\partial \boldsymbol{\delta}) \boldsymbol{M}_c$. If NDI is applied to the inner loop, the actuator deflections $\boldsymbol{\delta}$ can be solved by introducing a virtual input $\boldsymbol{\nu}_{\omega}$ to the inner loop, which yields

$$\boldsymbol{\delta} = (\boldsymbol{M}_c)_{\boldsymbol{\delta}}^{-1}(\boldsymbol{I} \boldsymbol{\nu}_{\omega} + \boldsymbol{\omega} \times \boldsymbol{I} \boldsymbol{\omega} - \boldsymbol{M}_a) \quad (9)$$

Similar to the outer loop, the introduction of a virtual input vector $\boldsymbol{\nu}_{\omega}$ yields a linear system $\dot{\boldsymbol{\omega}} = \boldsymbol{\nu}_{\omega}$, of which a linear controller is used to generate $\boldsymbol{\nu}_{\omega}$, depending on the errors between the measured and desired values of $\boldsymbol{\omega}$, as shown in Fig. 2.

It is noticed in Eq. (9) that the control law depends on the full aerodynamic model of \boldsymbol{M}_a and \boldsymbol{M}_c . However, due to the occurrence of damage, a lot of uncertainties are introduced to the aerodynamic model. Hence, the mismatch of the estimated \boldsymbol{M}_a will have an undesired impact on the performance of the NDI controller. Alternatively, the INDI method is used for inner loop to fix this issue. Consider only computing the increments of actuator deflections at each execution, which are only influenced by \boldsymbol{M}_c ; a large part of model uncertainties can be mitigated. The incremental part is obtained by a first-order Taylor approximation of $\dot{\boldsymbol{\omega}}$ in Eq. (7) [26]:

$$\begin{aligned} \dot{\omega} \approx \dot{\omega}_0 + \frac{\partial}{\partial \omega} [I^{-1}(\mathbf{M}_a - \omega \times I\omega)]_{\omega_0, \delta_0} (\omega - \omega_0) \\ + \frac{\partial}{\partial \delta} [I^{-1} \mathbf{M}_c]_{\omega_0, \delta_0} (\delta - \delta_0) \end{aligned} \quad (10)$$

where ω_0 and δ_0 are the measured values of the previous time step. Compared to the change of actuator deflections ($\delta - \delta_0$), the change of ω during a small increment of time is negligible, i.e., $\Delta\omega = (\omega - \omega_0) \approx 0$. This is a valid assumption because the angular rate ω is a continuous function of time, and its increment $\Delta\omega$ approaches zero as the time increment approaches zero. For the practical INDI controller we assume a “sufficiently high” sampling rate up to thousands of hertz, which guarantees that within less than 1 ms, the increment $\Delta\omega$ is indeed negligible. Hence, by denoting $(\delta - \delta_0)$ as $\Delta\delta$, Eq. (10) can be simplified as

$$\dot{\omega} \approx \dot{\omega}_0 + [I^{-1}(\mathbf{M}_c)_\delta] \Delta\delta \quad (11)$$

where $(\mathbf{M}_c)_\delta = (\partial \mathbf{M}_c / \partial \delta)$. It can be observed that a large part of the aerodynamic model \mathbf{M}_a is canceled since only the incremental form is considered. On the assumption of accurate sensor information of angular accelerations, the commanded incremental deflections of actuators can be solved by

$$\Delta\delta_{cmd} = (\mathbf{M}_c)_\delta^{-1} I(\nu_\omega - \dot{\omega}_0) \quad (12)$$

which yields the commanded control input to the aircraft:

$$\delta_{cmd} = \delta_0 + \Delta\delta_{cmd} \quad (13)$$

It should be noted that the derivation of the INDI method requires high-bandwidth actuators, and so the performance of the controller may degrade when the actuators are saturated due to system faults or aircraft damage, which will be discussed later in this paper.

IV. Case Study and Simulation Results

In this section, an online simulation of the complete envelope prediction and protection system (see Fig. 1) is conducted to investigate its online feasibility in given scenarios. The simulation is based on a model of the Cessna Citation aircraft, which is a twin-jet business aircraft shown in Fig. 3. The aircraft model is incorporated in a high-fidelity simulation environment in MATLAB Simulink for developing and testing new methodologies in a fly-by-wire system before they are implemented in real flight [36]. The simulation environment is called “DASMAT,” which is the acronym for the Delft University Aircraft Simulation Model and Analysis Tool. The Cessna Citation aircraft model and the DASMAT have been used in previous papers on flight-envelope calculation, damage modeling, and classification [21,22]. In this paper, databases of flight envelopes [22] are built in the form of lookup tables and incorporated in the DASMAT. Reachability analysis is chosen in this research as the technique to compute safe flight envelopes [16]. The computed results are called reachable sets, which are defined as a set of states that reach a certain target set within a given time horizon and current control authority [15,17]. The trim envelopes used in Ref. [13] are regarded as a target set when computing reachability-based flight envelopes.

To demonstrate the importance of envelope protection, two structural-damage cases are modeled in the DASMAT. The first case is symmetrical damage to the rudder, and the second case is asymmetrical damage to the left wing and aileron. The missing areas due to damage are contoured by red dashed lines in Fig. 3. The combination of both wing and rudder damage is also simulated and discussed. Figure 4 shows the flight envelopes retrieved from the database, which are used for online envelope update and protection. Obvious shrinkage of envelopes after each damage case can be observed in Fig. 4, which shows the influence of structural damage on the maneuverability of the impaired aircraft.

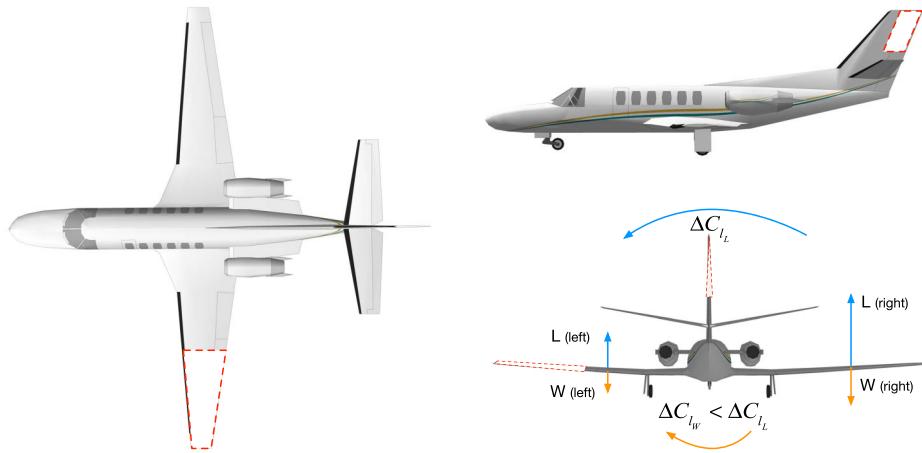


Fig. 3 A three-view illustration of a damaged Cessna Citation aircraft.

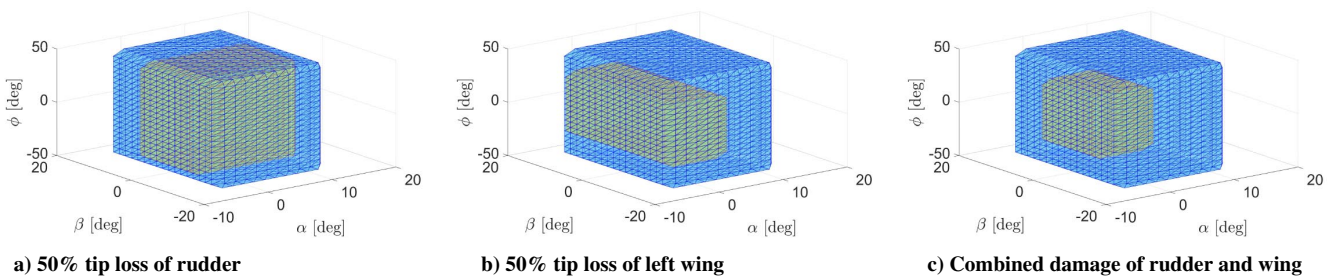


Fig. 4 Normal flight envelopes (blue) and their reduced forms after structural damage (green) retrieved from the database.

The simulations are performed in the DASMAT under normal and damage conditions. During each simulated flight, the aircraft is initially trimmed at the following flight conditions: the true airspeed $TAS = 100$ m/s and pressure altitude $H_p = 5000$ m with $\alpha = 3.7$. Sensor faults are not considered in this paper, and so all sensors are assumed to function normally.

A. Rudder Damage

The rudder and aileron are commonly used to maintain a zero sideslip angle to balance yawing moments and to generate sideslip, aligning the aircraft with the runway for crosswind landing. When lateral control is limited, the rudder can also be used as an alternative control effector for turning the aircraft [37]. In such a situation, the pilot/autopilot commands a rudder deflection to generate sideslip, leading to a rolling moment produced by the aircraft lateral static stability.

When the rudder is damaged, in order to maintain the same value of β , higher rudder deflection is required compared to the fully operational configuration. If the reference input is given without considering the reduced control effectiveness, the damaged rudder may soon saturate and lead to the loss of directional control. The aim of β protection is to prevent such aggressive use of the rudder and limit the maximum required rudder deflection to retain a directional authority margin in case of atmospheric disturbances.

As discussed in the previous section, the reidentification and classification form the primary phase of envelope prediction and protection. The reidentification is triggered when the errors between measured and modeled outputs exceed a certain threshold. The triggering threshold is predefined based on the lowest damage scale modeled in the simulation. For asymmetrical damage (e.g., wing damage), the reidentification signal is normally induced by unequal forces and increments of moments.

However, symmetrical damage, like tip loss of vertical tail and rudder, does not produce constant increments of yawing or rolling moment that triggers the reidentification. Nevertheless, it is still possible to detect the errors if the damaged rudder deflects to, for instance, maintain a nonzero β command. Additionally, reports on past flight accidents (e.g., American Airlines Flight 587, United Airlines Flight 585) reveal that rudder and vertical tail damage is often accompanied, or induced by sudden external disturbances and turbulence, when the rudder deflects to retrim the aircraft. Therefore, in the simulation, yawing moment disturbance is introduced as an input of the identification system.

For the online identification process, the recursive least-squares method has been implemented [9,22]. At each time instant, the covariance matrix gives some information of the reliability of the reidentified model parameters, which is closely related to the sufficiency of each state input. In abnormal situations, recovering and restabilizing maneuvers only excite a limited range of states, resulting in an updated local model of the current flight condition. By observing the variance

Table 1 Values of aerodynamic derivatives before and after 50% tip loss of rudder

	C_{n_β}	$C_{n_{\delta_r}}$	C_{n_r}
Original value	0.153	-0.1	-0.21
Value after damage	0.122	-0.05	-0.168

of each estimated parameter, it is found that not all parameters are identifiable. Nevertheless, the advantage of using classification is that it does not require all changed parameters to be accurately re-estimated, but only parameters that quickly converge are selected as classification features. This advantage naturally circumvents the safety concerns associated with obtaining global models in abnormal situations.

The classification is based on the neural-network (NN) method discussed in Ref. [21]. Two parameters, C_{n_β} and $C_{n_{\delta_r}}$, are selected as the classification features. They can either be trained as two individual features, which yield two separate classifiers, or as a feature set of one classifier. The advantage of using NN classification is that multiple classes can be trained in one classifier of the same classification features. Figure 5a shows the training result of three rudder-damage levels, which is quantified by percentage of tip loss.

Each data point for training, denoted by different markers in Fig. 5, is generated by system identification from each individual simulation test. The variance of training data in each class is caused by the variance in the level of external noise, the initial flight conditions, and the sufficiency of excitation inputs given in every simulation. It can be observed that the variance of C_{n_β} is larger than that of $C_{n_{\delta_r}}$, implying that the identification of $C_{n_{\delta_r}}$ is more sufficiently excited. Based on this training set, the classifier is more tolerant of the imprecise identification of C_{n_β} due to possible lack of sufficient excitation after damage.

In this section, a 50% loss of the rudder tip area is simulated by changing the values of aerodynamic terms in the lookup tables of the DASMAT simulation model. The original values of these parameters and their changed values after damage are listed in Table 1. The criteria applied to change these parameters are deduced from wind-tunnel results reported in Ref. [38].

In the simulation shown in Fig. 6, the rudder damage is triggered at 15 s. An impulse of external yaw moment ΔC_n is added at 15 s and lasts for 2 s to simulate the effect of disturbances and turbulence, which causes an immediate rise of the averaged errors of C_n . As shown in Fig. 6a, $\bar{\Delta C}_n$ exceeds the triggering threshold (3×10^{-7}) twice. Under the influence of an external yaw moment, β deviates from zero (Fig. 6b) and the rudder immediately deflects in response to the sudden change (Fig. 6c), which excites the identification of C_{n_β} and $C_{n_{\delta_r}}$, respectively. In Figs. 6e and 6f, the value of C_{n_β} changes from 0.147 to 0.12, and $C_{n_{\delta_r}}$ changes from -0.095 to -0.046 . It can

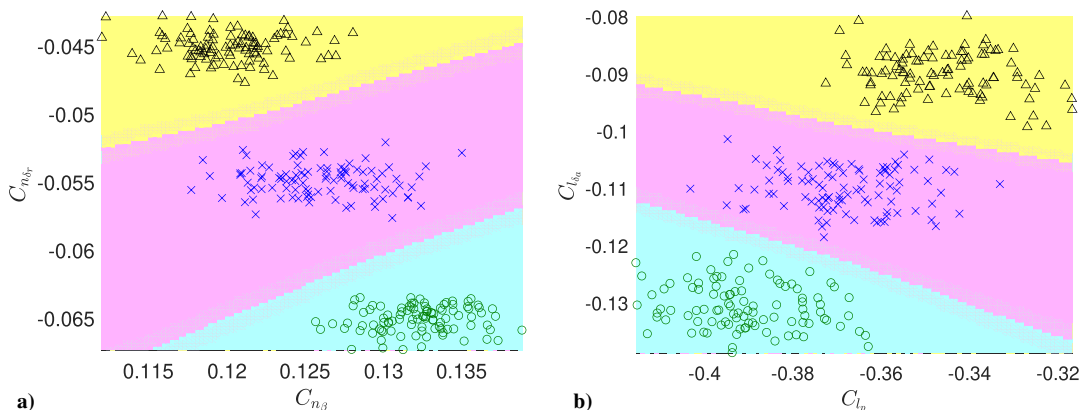


Fig. 5 Training result of a) rudder damage and b) wing damage using neural networks (damage levels of 30% are denoted by circles, of 40% are denoted by crosses, and of 50% are denoted by triangles).

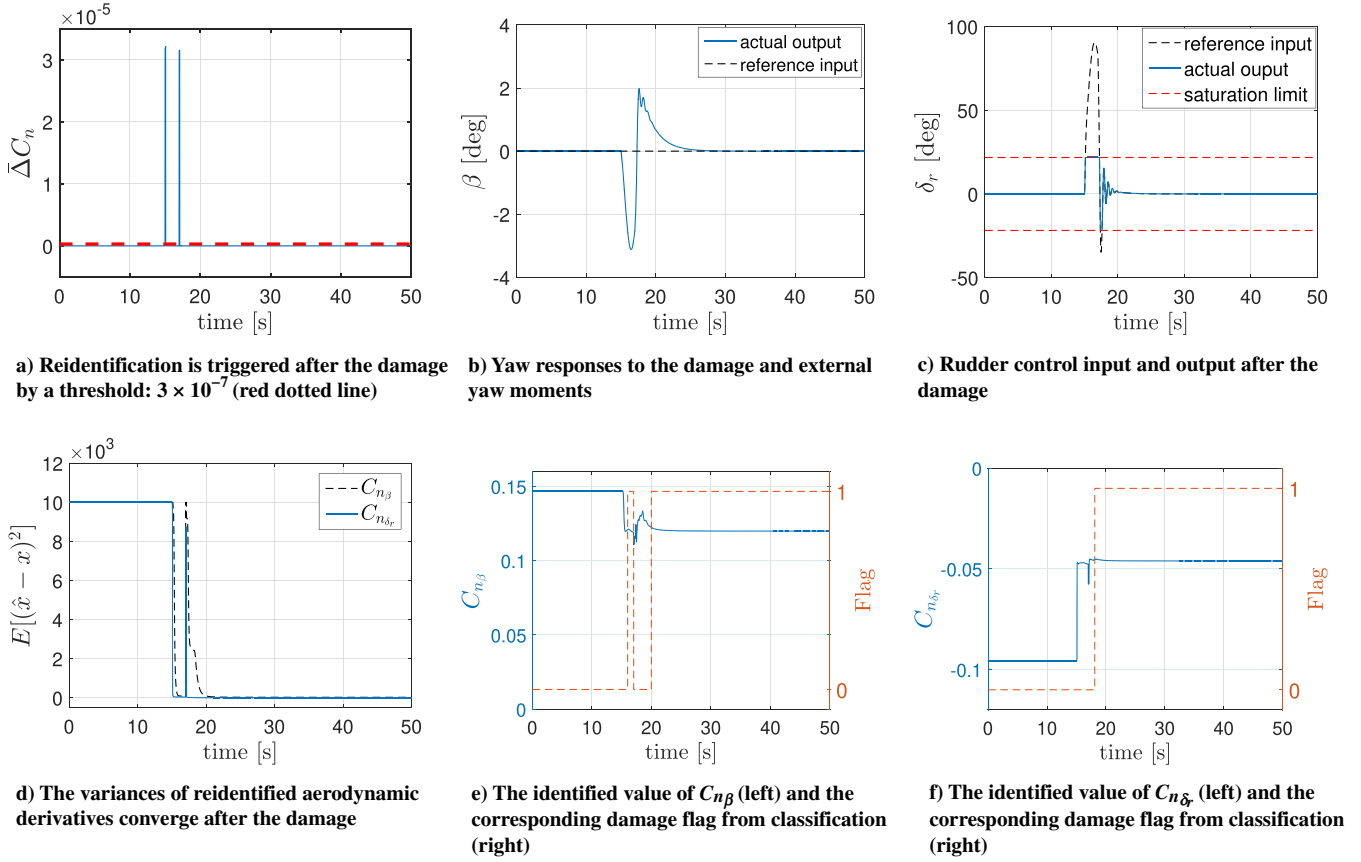


Fig. 6 Online identification and classification results of the rudder damage when the system is fully excited by large external yaw moments so that no further maneuvers are needed.

be observed from Fig. 6d that even though both parameters converge to their changed values, the variance of $C_{n\beta}$ converges a bit slower than that of $C_{n\delta_r}$. This is due to different excitation inputs of β and δ_r .

In the damage assessment system, each classifier corresponds to one damage case, and the output of each classifier is represented by an indication flag with the value of zero or one. Whichever flag becomes unity, its corresponding damage case is declared as the current damage case. In this simulation, the assessment system requires at least 50 converged samples to generate the classification flag, which is 50 s if the sampling rate is 100 Hz. Based on the identification results shown on the left axis, the flags of the expected damage case are shown on the right axes of Figs. 6e and 6f.

It can be observed from Fig. 6 that the system is fully excited by large external yaw moments so that no further maneuvers are needed to get the desired results. In the simulation shown in Fig. 7, the amplitude of the added impulse signal is reduced in order to simulate the situation where the restabilizing response of β is not enough to fully excite the identification of $C_{n\beta}$. As shown in Figs. 7b and 7c, at the time of damage occurrence β deviates from zero and the controller gives commands of δ_r to maintain zero sideslip angle, which generates the excitation inputs to the reidentification of $C_{n\beta}$ and $C_{n\delta_r}$. Figure 7d shows that before 20 s, the variance of the estimated $C_{n\beta}$ did not converge to a small value since the excitation of β is not sufficient. It is also observed that the transient of the damage flag is synchronized with the changes of variance, which is caused by the fluctuation of excitation input triggered by sudden damage or external disturbance.

From the perspective of identification, more β maneuvers are required for more accurate result, but this may also increase the risk of LOC in the current abnormal situation that has not yet been fully identified. Safety is always the first priority when it comes to flight, and so small maneuvers are suggested when giving excitation inputs. However, the criteria for “small maneuvers” are not numerically defined in literature. In this simulation, a limit of ± 2 for

β is suggested for the range of β maneuvers. The limit is based on the flight envelope of the most severe but still recoverable rudder-damage case retrieved from the database in order to prevent the aircraft from entering the LOC condition during the identification process.

As shown in Fig. 7, starting at 20 s, a series of the β command is manually given within the limits, which provides more excitation for the estimated $C_{n\beta}$ to approach its expected value around 25 s. It can be observed that under damage conditions, the uncertainty in the identification is magnified due to limited range of maneuvers and the insufficiency of excitation.

Since the estimated variance provides a convenient metric for assessing whether $C_{n\beta}$ can be adequately identified, the decision will be made based on the value of its variance of estimation. If the variance is under a certain threshold, it means that the estimation is close to the expected value. Given the high generalization ability of pattern classification, even a moderately accurate $C_{n\beta}$ can still generate the expected classification results, as shown in Fig. 7e. If the variance of estimation remains at a value above the threshold, it means that the estimated $C_{n\beta}$ deviates too far from the expected value and cannot be included as a feature input in the classification. Under this condition, the classification will only depend on the identification of $C_{n\delta_r}$, which converges more easily since rudder deflections δ_r in the inner loop have faster dynamics, and thus generate sufficient excitation.

The comparison between flights with and without updated β protection after rudder damage is shown in Fig. 8. Before damage occurs, the sideslip angle β is maintained at around -5 . At the time of damage (15 s), the value of rudder deflections suddenly increases, which is necessary to maintain the same value of β and generates the errors shown in Fig. 8a. Based on the identified $C_{n\delta_r}$, rudder damage is quickly classified and confirmed after the damage. As shown in Figs. 8b and 8c, at 20 s, the reference input for β continues to increase until the damaged rudder begins to saturate. It is observed from Fig. 8b

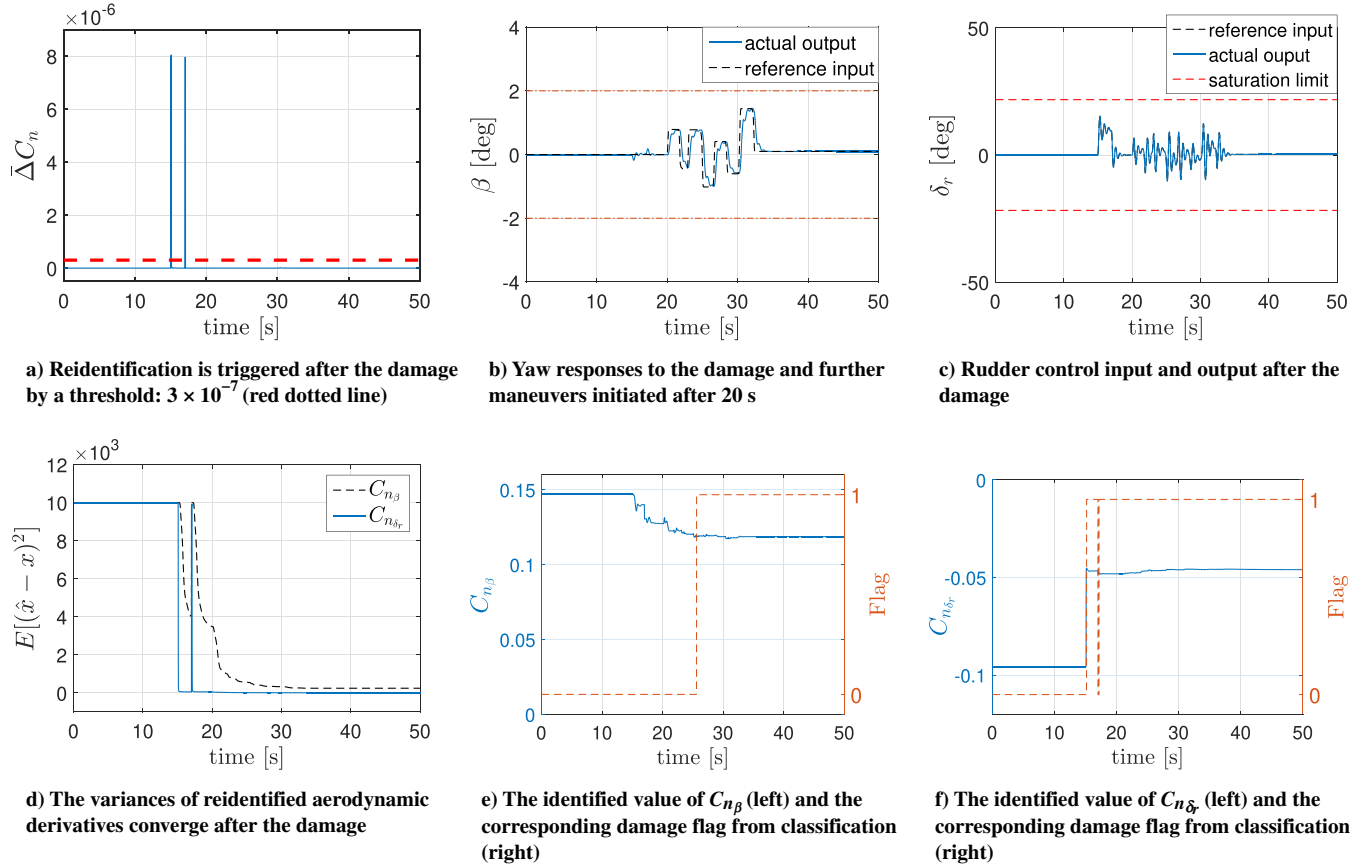


Fig. 7 Online identification and classification results of the rudder damage when the system is not fully excited by small external yaw moments so that further maneuvers are initiated.

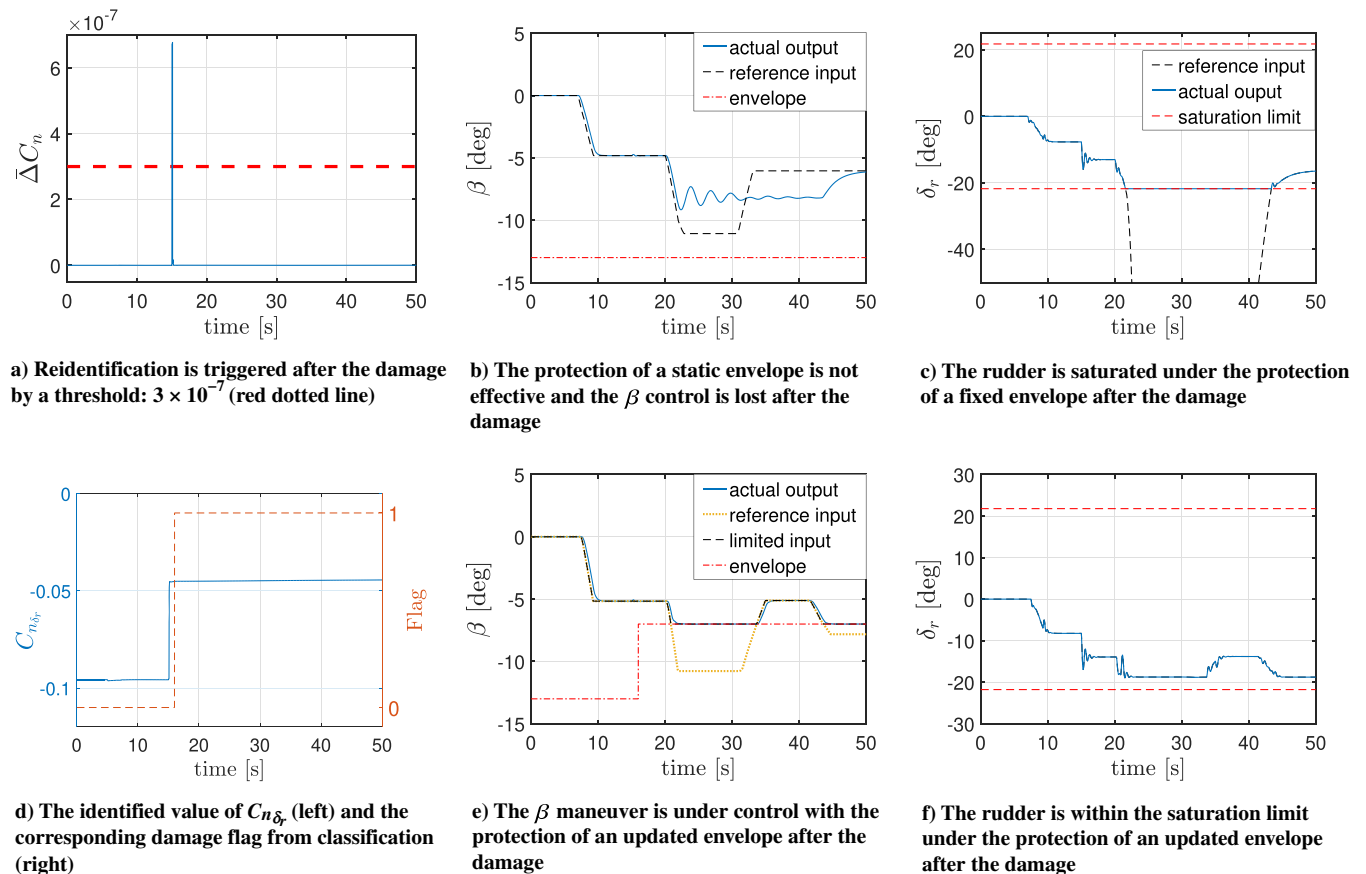


Fig. 8 Comparisons of β control between static and online updated flight-envelope protections after 50% tip loss of rudder.

that excessive β commands are given because of the lack of the information on the new limit so that the aircraft is under the protection of a static envelope. Due to the saturation of rudder deflection shown in Fig. 8c, the directional control in Fig. 8b is not regained until after 42 s, which is more than 10 s after the β command is reduced at 30 s. Even though rudder deflection saturation is not expected to produce unbalanced rolling moments if lateral control effectiveness is not reduced, strong forces at extreme positions may trigger more severe damage, like the total loss of the rudder and vertical stabilizer. In addition, control effector saturation by itself can be a precursor to LOC, which means it should be avoided at all times. With updated information of the changed envelope shown in Fig. 4a, the same excessive input command is limited within the bounds of the online updated envelope, as shown in Figs. 8e and 8f, which makes sure that the rudder deflections are always kept within the saturation limit.

B. Left Wing and Aileron Damage

Unlike rudder damage, wing damage is asymmetrical, generating an incremental rolling moment ΔC_l from the unequal lift force ΔC_{l_L} and weight ΔC_{l_w} , as shown in the lower right subplot of Fig. 3. Since the reduction of weight is much less compared to lift force, its contribution to ΔC_l is neglected.

Figure 9 shows data from NASA wind-tunnel experiments conducted on a generic fixed-wing aircraft model with 50% tip loss of the left wing [38], which indicates how incremental rolling moments change with angle of attack under wing damage. It is observed that ΔC_l can be approximated by a linear function of α in low-angle-of-attack regions between $\alpha = -5$ and $\alpha = 10$. Hence, ΔC_l in the DASMAT can be modeled as

$$\Delta C_l = C_{l_\alpha} \cdot \alpha \quad (14)$$

It should be noted that the coefficient C_{l_α} defined in this equation is different from conventional C_{l_α} . It can be regarded as a disturbance factor under wing damage. As indicated by the wind-tunnel tests [38], the damage also induces reduction in the stability and control authority of the aircraft, which is reflected in the changed values of aerodynamic derivatives like the control effectiveness $C_{l_{\delta_a}}$ and roll damping C_{l_p} . The changes of C_{l_α} , $C_{l_{\delta_a}}$, and C_{l_p} are modeled in the DASMAT to simulate the influence of the damage. In this example, a damage case of 50% tip loss of the left wing is simulated. Table 2 lists the original values of these significantly influenced aerodynamic derivatives in the lookup table and their modeled values after damage.

Similar to the rudder damage, the classification training is also based on two features, which are $C_{l_{\delta_a}}$ and C_{l_p} . It should be noted that even though C_{l_α} also changes after damage, it is not necessarily included as a classification feature since the reidentification of this parameter may require maneuvers producing a large amplitude of perturbation with respect to α , which poses potential risk to the damaged aircraft.

Table 2 Values of aerodynamic derivatives before and after 50% tip loss of left wing

	C_{l_p}	$C_{l_{\delta_a}}$	C_{l_α}
Original value	-0.46	-0.186	0
Value after damage	-0.345	-0.093	0.6

Figure 5b shows the training result for $C_{l_{\delta_a}}$ and C_{l_p} of three different levels of wing damage to be used in the classification.

As shown in Fig. 10a, the damage is initiated at 5 s; and the averaged error of the incremental rolling moment $\overline{\Delta C_l}$ suddenly increases above the threshold, which triggers the reidentification. Sufficient excitation for identification is less of an issue compared to rudder damage due to the existence of the incremental rolling moment. In response to the sudden roll motion at 5 s (Fig. 10b), the undamaged (right) aileron deflects in an effort to retrim the aircraft and compensate for the incremental moment ΔC_l , as shown in Fig. 10c. Meanwhile, the aileron deflections and roll motions have provided sufficient excitation inputs to the reidentification of aerodynamic derivatives, as can be observed from the variance convergence in Fig. 10d. The identified C_{l_p} and $C_{l_{\delta_a}}$ are shown on the left axis of Figs. 10e and 10f, and the classification results are shown on the right.

As shown in Figs. 10b and 10c, the first aileron deflection overshoot at a time of $t = 5$ s corresponds to the maximum control surface deflection. In the course of restabilizing the aircraft, the aileron needs to deflect about 25 deg to keep the aircraft at steady state after the Dutch roll is completely damped, leaving limited authority (13 deg) for further roll control. If ΔC_l continues to increase, the right aileron will saturate and the aircraft may enter into LOC if airspeed does not increase within a short period of time.

According to the previous analysis of wing damage and Eq. (14), the increase of α may generate too much rolling moment, saturating the actuator and leading to uncontrollable roll motions. Under normal conditions without damage, as shown in Fig. 11a, the angle of attack can be controlled to increase to above 8 deg during pitch maneuvers, and the roll motion is barely influenced (Fig. 11d) due to the decoupled effect of α . In the wing damage scenario shown in Fig. 11b, the command of α starts to increase at 30 s after the damaged aircraft has been retrimmed. Under the coupled influence of wing damage, the value of aileron deflection δ_a increases with α (Fig. 11e) to compensate for the rolling moment. As shown in Figs. 11b and 11e, α increases to about 5.5 deg when δ_a meets the upper limit and the aircraft starts rolling to one side under the incremental rolling moment that cannot be counteracted. This indicates that the protection of static flight envelopes no longer works and the angle of attack needs to be controlled within the updated envelope so that the damaged aircraft is not subjected to an uncontrollable rolling moment.

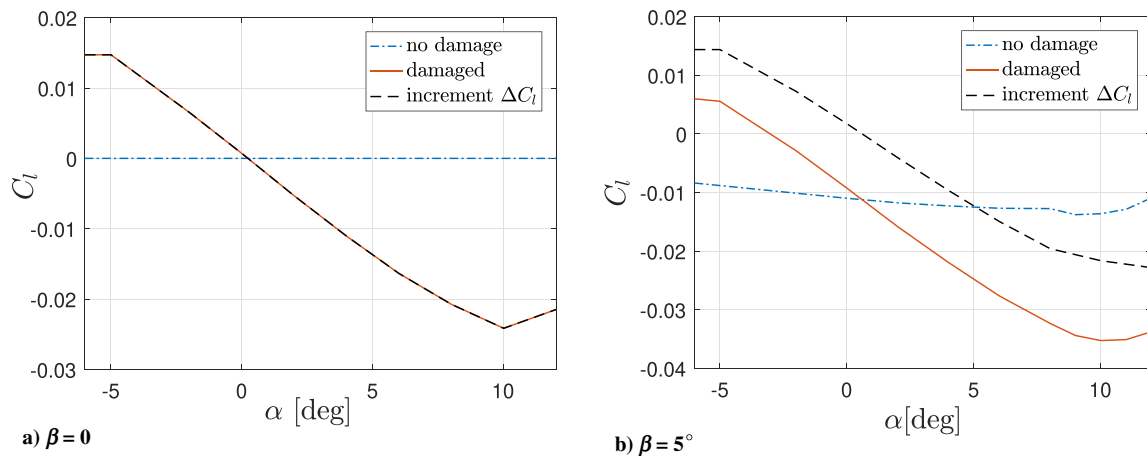


Fig. 9 Wind-tunnel data of incremental rolling moment with respect to angle of attack.

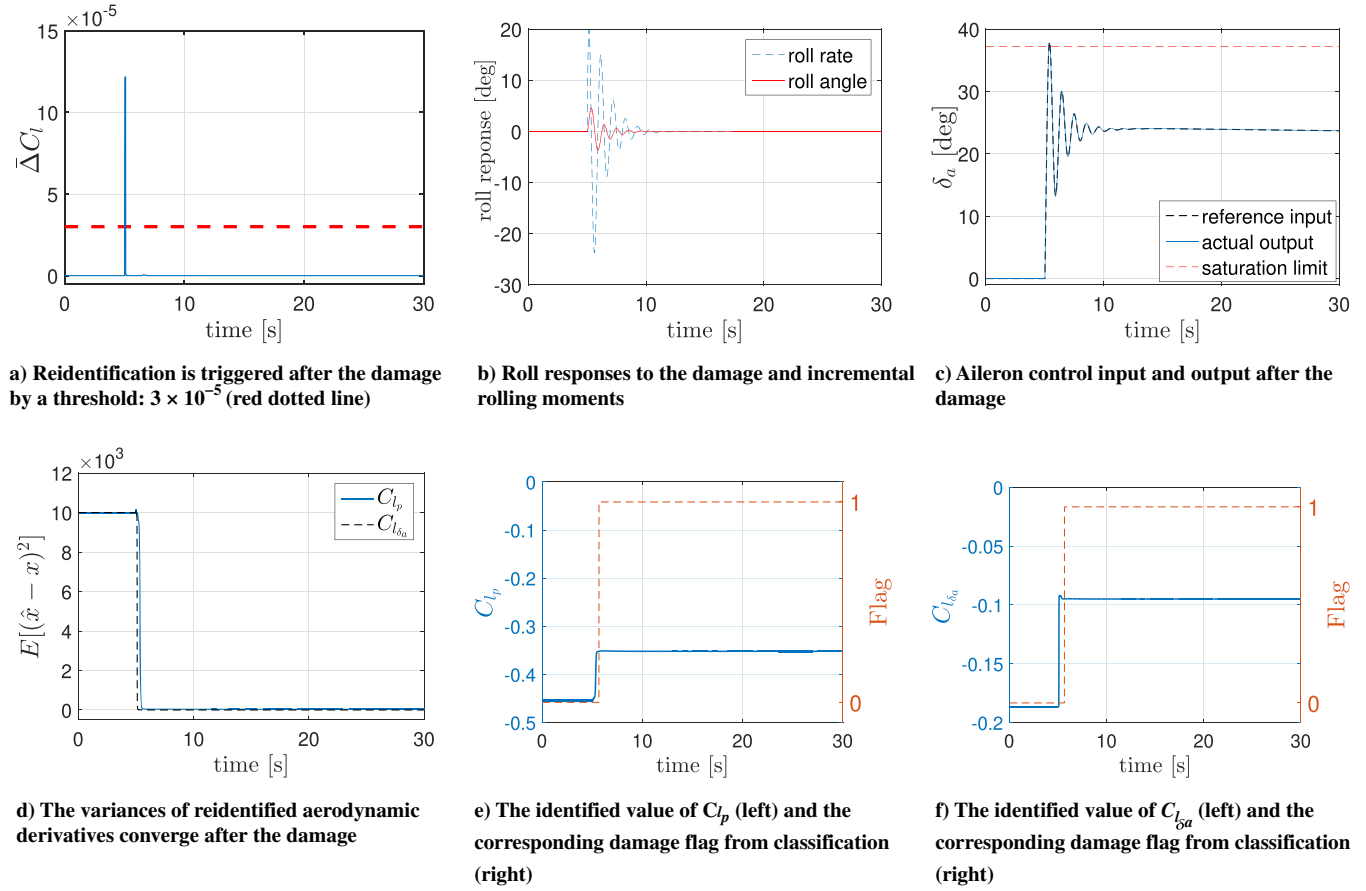


Fig. 10 Online identification and classification results of the wing damage.

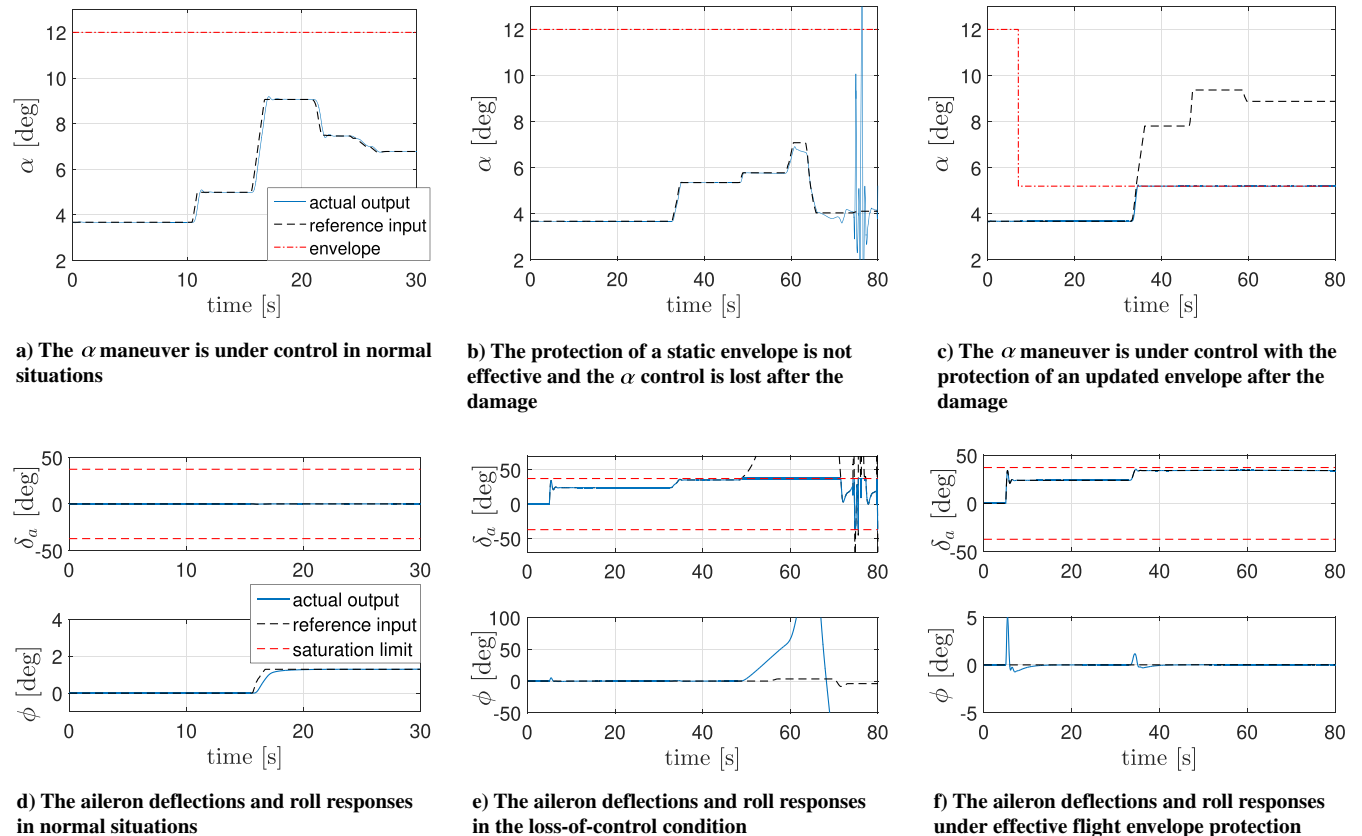


Fig. 11 Comparisons of α control between static and online updated flight-envelope protections after 50% wing-tip loss.

The flight under envelope protection is shown in the third column of Fig. 11, where the updated envelope is retrieved based on the current damage case and flight states (see Fig. 4b). The reference input of α given by pilots/autopilot is not directly sent to the controller but restricted by the retrieved envelope to about 5.2 deg before the deflection of δ_a is computed by the INDI controller. As shown in Fig. 11f, δ_a is kept within the limit so that there is no unwanted rolling motion during pitching maneuvers and the damaged aircraft is always under control.

C. Combined Rudder and Wing Damage

In this example, both the left wing and the rudder are damaged at 5 and 15 s, respectively, which results in combined aerodynamic effect on the aircraft where the updated envelopes of both α and β are needed.

In the simulation shown in Fig. 12a, the aircraft is well protected after the wing damage occurs at 5 s with the updated flight envelope. However, the situation of wing damage deteriorates after the occurrence of rudder damage, and the single α -envelope protection is no longer effective.

In case of single damage of the rudder, as previously shown in Fig. 8b, the saturation will cause deviations from the commanded β but not total LOC of the aircraft. However, when rudder damage is combined with wing damage, the envelope protection of β becomes critical due to the coupling between directional and lateral motions.

As shown in Fig. 12b, after the rudder is damaged at 15 s, the flight envelope is not updated and the increasing command of β is not limited. At around 20 s, the control of β is lost without effective β -envelope protection and the rudder is saturated (Fig. 12c). The uncontrolled yaw motion generates more rolling moments that require additional aileron deflections. Meanwhile, in the extreme situation shown in Fig. 12a, the α command has gone beyond the safe limit, the actual α is maintained within the envelope boundary, and the aileron deflection is at the edge of saturation before 20 s. Therefore, when both the ailerons and rudder are saturated, the additional rolling

moment cannot be mitigated by the remaining control authorities, which causes the aircraft to roll to one side and become unrecoverable.

It can be concluded that in the situation of combined damage, the protection of α can no longer prevent the aircraft from LOC if β is not effectively protected. The flight envelope of the combined damage in Fig. 4c is stored in the database and retrieved to replace and update the normal static envelope once the damage is identified. As shown in Fig. 12e, the envelope boundary for β protection has changed. It can be observed from the second row of Fig. 12 that the utilization of both β and α envelope protection can effectively prevent a LOC situation when excessive commands are given to the controller after the damage.

D. Discussion

Among all the LOC hazards that have a fundamental influence on flight envelopes, structural damage discussed in this paper is only one category. Combination with other abnormal cases can lead to further changes of flight envelopes and more stringent protection strategies. For example, icing-induced LOC incidents and accidents have occurred on all classes of aircraft [39,40]. The primary aerodynamic effect of icing is the increased drag force and reduced lift force on the icing part. Normally, ice accretion is not symmetrical, thus inducing moments from unequal forces. Based on this analysis, icing can be regarded as a modification of the airframe outline, and its aerodynamic impact is similar to that of structural damage discussed in this paper. Due to the lack of aerodynamic modeling data, icing is not modeled and simulated in this paper.

It should also be noted that the cooperation between pilots and the automatic controller plays a vital role in some complicated situations like engine failures and actuator faults [14,37]. Besides, it is possible that a reference input, potentially attenuated by flight-envelope protection, leads to the condition of controlled flight into terrain. Therefore, future improvement work can be focused on using flight envelopes and terrain data in the warning system to enhance the situational awareness of the pilot and to improve the efficiency of human-machine interactions.

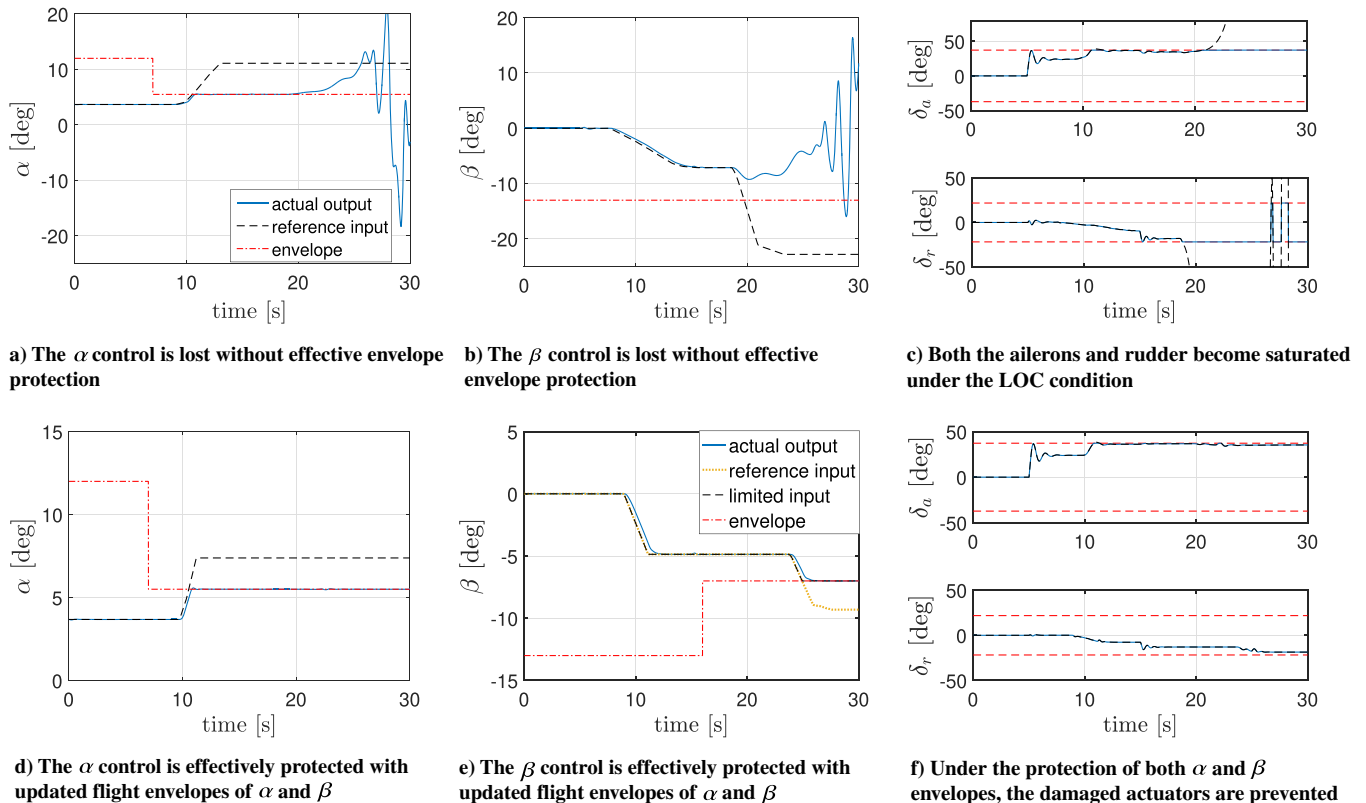


Fig. 12 In the situation of combined damage, LOC can be prevented only if both α and β envelopes are updated and protected.

V. Conclusions

A flight-envelope protection system with online-updated envelope information is developed in this paper. The system is implemented online in a closed loop, combining fault-tolerant flight control, system identification, damage assessment, and database retrieval. Three in-flight damage cases are conducted in the simulation to test the performance of the flight-envelope protection system. In addition, practical issues about insufficient excitation for system identification under damage are addressed in the simulation. The test results indicate that the proposed system can effectively help prevent the damaged aircraft from flying into loss-of-control conditions.

References

- [1] Tekles, N., Chongvisal, J., Xargay, E., Choe, R., Talleur, D. A., Hovakimyan, N., and Belcastro, C. M., "Design of a Flight Envelope Protection System for NASA's Transport Class Model," *Journal of Guidance, Control, and Dynamics*, Vol. 40, No. 4, 2017, pp. 863–877. <https://doi.org/10.2514/1.G001728>
- [2] Lee, H., Snyder, S., and Hovakimyan, N., "L1 Adaptive Control Within a Flight Envelope Protection System," *Journal of Guidance, Control, and Dynamics*, Vol. 40, No. 4, 2017, pp. 1013–1026. <https://doi.org/10.2514/1.G001742>
- [3] Briere, D., and Traverse, P., "AIRBUS A320/A330/A340 Electrical Flight Controls—A Family of Fault-Tolerant Systems," *FTCS-23: The Twenty-Third International Symposium on Fault-Tolerant Computing*, IEEE, New York, 1993, pp. 616–623. <https://doi.org/10.1109/FTCS.1993.627364>
- [4] Ackerman, K. A., Talleur, D. A., Carbonari, R. S., Xargay, E., Seefeldt, B. D., Kirlik, A., Hovakimyan, N., and Trujillo, A. C., "Automation Situation Awareness Display for a Flight Envelope Protection System," *Journal of Guidance, Control, and Dynamics*, Vol. 40, No. 4, 2017, pp. 964–980. <https://doi.org/10.2514/1.G000338>
- [5] Lombaerts, T. J. J., Loooye, G., Ellerbroek, J., and Martin, M. R. Y., "Design and Piloted Simulator Evaluation of Adaptive Safe Flight Envelope Protection Algorithm," *Journal of Guidance, Control, and Dynamics*, Vol. 40, No. 8, 2017, pp. 1902–1924. <https://doi.org/10.2514/1.G002525>
- [6] Van Baelen, D., Ellerbroek, J., van Paassen, M. M., and Mulder, M., "Design of a Haptic Feedback System for Flight Envelope Protection," *AIAA Modeling and Simulation Technologies Conference*, AIAA Paper 2018-0117, 2018. <https://doi.org/10.2514/6.2018-0117>
- [7] Ellerbroek, J., Martin, M. J., Lombaerts, T. J. J., van Paassen, M. M., and Mulder, M., "Design and Evaluation of a Flight Envelope Protection Haptic Feedback System," *IFAC-PapersOnLine*, Vol. 49, No. 19, 2016, pp. 171–176. <https://doi.org/10.1016/j.ifacol.2016.10.481>
- [8] Chowdhary, G., Johnson, E. N., Chandramohan, R., Kimbrell, M. S., and Calise, A., "Guidance and Control of Airplanes Under Actuator Failures and Severe Structural Damage," *Journal of Guidance, Control, and Dynamics*, Vol. 36, No. 4, 2013, pp. 1093–1104. <https://doi.org/10.2514/1.58028>
- [9] Lombaerts, T., Huisman, H., Chu, P., Mulder, J. A., and Joosten, D., "Nonlinear Reconfiguring Flight Control Based on Online Physical Model Identification," *Journal of Guidance, Control, and Dynamics*, Vol. 32, No. 3, 2009, pp. 727–748. <https://doi.org/10.2514/1.40788>
- [10] Wilborn, J. E., and Foster, J. V., "Defining Commercial Transport Loss-of-Control: A Quantitative Approach," *AIAA Atmospheric Flight Mechanics Conference*, AIAA Paper 2004-4811, 2004. <https://doi.org/10.2514/6.2004-4811>
- [11] Chongvisal, J., Tekles, N., Xargay, E., Talleur, D., Kirlik, A., and Hovakimyan, N., "Loss-of-Control Prediction and Prevention for NASA's Transport Class Model," *AIAA Guidance, Navigation, and Control Conference*, AIAA Paper 2014-0784, 2014. <https://doi.org/10.2514/6.2014-0784>
- [12] Tekles, N., Holzapfel, F., Xargay, E., Choe, R., Hovakimyan, N., and Gregory, I. M., "Flight Envelope Protection for NASA's Transport Class Model," *AIAA Guidance, Navigation, and Control Conference*, AIAA Paper 2014-0269, 2014. <https://doi.org/10.2514/6.2014-0269>
- [13] Tang, Y., Atkins, E., and Sanner, R., "Emergency Flight Planning for a Generalized Transport Aircraft with Left Wing Damage," *AIAA Guidance, Navigation and Control Conference and Exhibit*, AIAA Paper 2007-6873, 2007. <https://doi.org/10.2514/6.2007-6873>
- [14] Di Donato, P. F. A., Balachandran, S., McDonough, K., Atkins, E. M., and Kolmanovsky, I., "Envelope-Aware Flight Management for Loss of Control Prevention Given Rudder Jam," *Journal of Guidance, Control, and Dynamics*, Vol. 40, No. 4, 2017, pp. 1027–1041. <https://doi.org/10.2514/1.G000252>
- [15] Fedkiw, R., and Osher, S., *Level Set Methods and Dynamic Implicit Surfaces*, Springer, New York, 2003, pp. 47–54, <http://link.springer.com/content/pdf/10.1007/b98879.pdf>.
- [16] Lygeros, J., "On Reachability and Minimum Cost Optimal Control," *Automatica*, Vol. 40, No. 6, 2004, pp. 917–927. <https://doi.org/10.1016/j.automatica.2004.01.012>
- [17] Mitchell, I. M., Bayen, A. M., and Tomlin, C. J., "A Time-Dependent Hamilton-Jacobi Formulation of Reachable Sets for Continuous Dynamic Games," *IEEE Transactions on Automatic Control*, Vol. 50, No. 7, 2005, pp. 947–957. <https://doi.org/10.1109/TAC.2005.851439>
- [18] Kaynama, S., Mitchell, I. M., Oishi, M., and Dumont, G. A., "Scalable Safety-Preserving Robust Control Synthesis for Continuous-Time Linear Systems," *IEEE Transactions on Automatic Control*, Vol. 60, No. 11, 2015, pp. 3065–3070. <https://doi.org/10.1109/TAC.2015.2411872>
- [19] Van Oort, E. R., "Adaptive Backstepping Control and Safety Analysis for Modern Fighter Aircraft," Ph.D. Thesis, Delft Univ. of Technology, Delft, The Netherlands, 2011.
- [20] Lombaerts, T., Schuet, S., Acosta, D., Kaneshige, J., Shish, K., and Martin, L., "Piloted Simulator Evaluation of Safe Flight Envelope Display Indicators for Loss of Control Avoidance," *Journal of Guidance, Control, and Dynamics*, Vol. 40, No. 4, 2017, pp. 948–963. <https://doi.org/10.2514/1.g001740>
- [21] Zhang, Y., de Visser, C. C., and Chu, Q. P., "Aircraft Damage Identification and Classification for Database-Driven Online Flight-Envelope Prediction," *Journal of Guidance, Control, and Dynamics*, Vol. 41, No. 2, 2018, pp. 449–460. <https://doi.org/10.2514/1.G002866>
- [22] Zhang, Y., de Visser, C. C., and Chu, Q. P., "Database Building and Interpolation for an Online Safe Flight Envelope Prediction System," *Journal of Guidance, Control, and Dynamics*, Vol. 42, No. 5, 2019, pp. 1166–1174. <https://doi.org/10.2514/1.G003834>
- [23] Patton, R. J., "Fault-Tolerant Control: The 1997 Situation," *Proceedings of the IFAC Symposium SAFEPROCESS 97*, 1997, pp. 1033–1055. [https://doi.org/10.1016/S1474-6670\(17\)42536-5](https://doi.org/10.1016/S1474-6670(17)42536-5)
- [24] Zhang, Y., and Jiang, J., "Bibliographical Review on Reconfigurable Fault-Tolerant Control Systems," *Annual Reviews in Control*, Vol. 32, No. 2, 2008, pp. 229–252. <https://doi.org/10.1016/j.arcontrol.2008.03.008>
- [25] Bacon, B., Ostroff, A. J., and Joshi, S., "Reconfigurable NDI Controller Using Inertial Sensor Failure Detection & Isolation," *IEEE Transactions on Aerospace and Electronic Systems*, Vol. 37, No. 4, 2001, pp. 1373–1383. <https://doi.org/10.1109/7.976972>
- [26] Sieberling, S., Chu, Q. P., and Mulder, J. A., "Robust Flight Control Using Incremental Nonlinear Dynamic Inversion and Angular Acceleration Prediction," *Journal of Guidance, Control, and Dynamics*, Vol. 33, No. 6, 2010, pp. 1732–1742. <https://doi.org/10.2514/1.49978>
- [27] Tol, H. J., Visser, C. C. D., Sun, L. G., Kampen, E. V., and Chu, Q. P., "Multivariate Spline-Based Adaptive Control of High-Performance Aircraft with Aerodynamic Uncertainties," *Journal of Guidance, Control, and Dynamics*, Vol. 39, No. 4, 2016, pp. 781–800. <https://doi.org/10.2514/1.G001079>
- [28] Smeur, E. J. J., Chu, Q., and de Croon, G. C. H. E., "Adaptive Incremental Nonlinear Dynamic Inversion for Attitude Control of Micro Air Vehicles," *Journal of Guidance, Control, and Dynamics*, Vol. 39, No. 3, 2016, pp. 450–461. <https://doi.org/10.2514/1.G001490>
- [29] Sun, S., Sijbers, L., Wang, X., and de Visser, C. C., "High-Speed Flight of Quadrotor Despite Loss of Single Rotor," *IEEE Robotics and Automation Letters*, Vol. 3, No. 4, 2018, pp. 3201–3207. <https://doi.org/10.1109/LRA.2018.2851028>
- [30] Simplício, P., Pavel, M. D., van Kampen, E., and Chu, Q. P., "An Acceleration Measurements-Based Approach for Helicopter Nonlinear Flight Control Using Incremental Nonlinear Dynamic Inversion," *Control Engineering Practice*, Vol. 21, No. 8, 2013, pp. 1065–1077. <https://doi.org/10.1016/j.conengprac.2013.03.009>
- [31] Matamoros, I., and de Visser, C. C., "Incremental Nonlinear Control Allocation for a Tailless Aircraft with Innovative Control Effectors," *AIAA Guidance, Navigation, and Control Conference*, AIAA Paper 2018-1116, 2018. <https://doi.org/10.2514/6.2018-1116>

- [32] Lu, P., van Kampen, E. J., de Visser, C., and Chu, Q., "Aircraft Fault-Tolerant Trajectory Control Using Incremental Nonlinear Dynamic Inversion," *Control Engineering Practice*, Vol. 57, Dec. 2016, pp. 126–141. <https://doi.org/10.1016/j.conengprac.2016.09.010>
- [33] Grondman, F., Looye, G., Kuchar, R. O., Chu, Q. P., and Van Kampen, E.-J., "Design and Flight Testing of Incremental Nonlinear Dynamic Inversion-Based Control Laws for a Passenger Aircraft," *2018 AIAA Guidance, Navigation, and Control Conference*, AIAA Paper 2018-0385, 2018. <https://doi.org/10.2514/6.2018-0385>
- [34] Falkena, W., Borst, C., Chu, Q., and Mulder, J., "Investigation of Practical Flight Envelope Protection Systems for Small Aircraft," *Journal of Guidance, Control, and Dynamics*, Vol. 34, No. 4, 2011, pp. 976–988. <https://doi.org/10.2514/1.53000>
- [35] Tol, H. J., de Visser, C. C., van Kampen, E., and Chu, Q. P., "Nonlinear Multivariate Spline-Based Control Allocation for High-Performance Aircraft," *Journal of Guidance, Control, and Dynamics*, Vol. 37, No. 6, 2014, pp. 1840–1862. <https://doi.org/10.2514/1.g000065>
- [36] Van Der Linden, C. A. A. M., *DASMAT-Delft University Aircraft Simulation Model and Analysis Tool: A Matlab/Simulink Environment for Flight Dynamics and Control Analysis.*, Delft Univ. of Technology, Delft, The Netherlands, 1996, pp. 23–50.
- [37] Koolstra, H., "Preventing Loss of Aircraft Control: Aiding Pilots in Manual Recovery from Roll-Limited Situations," Ph.D. Thesis, Delft Univ. of Technology, Delft, The Netherlands, 2017.
- [38] Shah, G. H., "Aerodynamic Effects and Modeling of Damage to Transport Aircraft," *AIAA Guidance, Navigation and Control Conference and Exhibit*, AIAA Paper 2008-6203, 2008, . <https://doi.org/10.2514/6.2008-6203>
- [39] Lombaerts, T., Looye, G., Seefried, A., Neves, M., and Bellmann, T., "Proof of Concept Simulator Demonstration of a Physics Based Self-Preserving Flight Envelope Protection Algorithm," *Engineering Applications of Artificial Intelligence*, Vol. 67, Jan. 2018, pp. 368–380. <https://doi.org/10.1016/j.engappai.2017.08.014>
- [40] Gingras, D., Ranaudo, R., Barnhart, B., Ratvasky, T., and Morelli, E., "Envelope Protection for In-Flight Ice Contamination," *AIAA Aerospace Sciences Meeting*, AIAA Paper 2009-1458, 2009. <https://doi.org/10.2514/6.2009-1458>

E. Atkins
Associate Editor